Journal of Instrumentation

OPEN ACCESS

Development of a New Class of Scintillating Fibres with Very Short Decay Time and High Light Yield

To cite this article: O. Borshchev *et al* 2017 *JINST* **12** P05013

View the article online for updates and enhancements.

Related content

- Single crystalline LuAG fibers for homogeneous dual-readout calorimeters
K Pauwels, C Dujardin, S Gundacker et al.
- Strip detectors for a portal monitor application
G.V. Russo, D. Lo Presti, D. Bonanno et al.
- A large Scintillating Fibre Tracker for LHCb
R. Greim

This content was downloaded from IP address 131.169.4.70 on 08/12/2017 at 12:08

Published by IOP Publishing for Sissa Medialab

Received: *March 22, 2017*
Accepted: *May 11, 2017*
Published: *May 17, 2017*

Development of a New Class of Scintillating Fibres with Very Short Decay Time and High Light Yield

O. Borshchev,[a] **A.B.R. Cavalcante,**[b] **L. Gavardi,**[c,1] **L. Gruber,**[d] **C. Joram,**[d] **S. Ponomarenko,**[a] **O. Shinji**[e] **and N. Surin**[a]

[a] *Enikolopov Institute of Synthetic Polymeric Materials of the Russian Academy of Sciences, Moscow 117393, Russian Federation*
[b] *CBPF, Rio de Janeiro, Brazil*
[c] *Technische Universität Dortmund, D-44221 Dortmund, Germany*
[d] *CERN, PH Department, CH-1211 Geneva 23, Switzerland*
[e] *Kuraray CO., LTD., Methacrylate Development Department, Tokyo, 100-8115, Japan*

E-mail: laura.gavardi@cern.ch

Abstract: We present first studies of a new class of scintillating fibres which are characterised by very short decay times and high light yield. The fibres are based on a novel type of luminophores admixed to a polystyrene core matrix. These so-called Nanostructured Organosilicon Luminophores (NOL) have high photoluminescense quantum yield and decay times just above 1 ns. A blue and a green emitting prototype fibre with 250 μm diameter were produced and characterised in terms of attenuation length, ionisation light yield, decay time and tolerance to x-ray irradiation. The well-established Kuraray SCSF-78 and SCSF-3HF fibres were taken as references. Even though the two prototype fibres mark just an intermediate step in an ongoing development, their performance is already on a competitive level. In particular, their decay time constants are about a factor of two shorter than the fastest known fibres, which makes them promising candidates for time critical applications.

Keywords: Scintillators, scintillation and light emission processes (solid, gas and liquid scintillators); Calorimeters; Particle tracking detectors; Timing detectors

[1] Corresponding author.

© CERN 2017, published under the terms of the Creative Commons Attribution 3.0 License by IOP Publishing Ltd and Sissa Medialab srl. Any further distribution of this work must maintain attribution to the author(s) and the published article's title, journal citation and DOI.

doi:10.1088/1748-0221/12/05/P05013

Contents

2017 JINST 12 P05013

1 Introduction

1.1 Scintillating fibres

The use of plastic scintillating fibres (PSF or SciFi) as active elements of particle detectors or active targets has a more than 30 years long history in nuclear and high energy physics. The SciFi technology allows building intrinsically fast, low mass tracking detectors with a high degree of geometrical adaptability [1, 2]. A further vast field of application is calorimetry, both electromagnetic and hadronic, where scintillating fibres are embedded in a high-Z absorber medium (typically lead) [3, 4]. Scintillating fibres can also be arranged as active targets, providing fast trigger and/or high resolution 3D vertexing [5].

The technological evolution and performance of scintillating fibre based detectors is tightly linked to the photodetection technology, currently culminating in the so-called Silicon Photomultiplier (SiPM) [6], which revived the interest in the SciFi technology and has opened up new fields of applications. The intrinsic properties of the SiPM, in particular the combination of high sensitivity, high gain and fast pulse shape, implemented in a solid-state sensor of sub-mm^2 size, allow for designing large-scale high-resolution SciFi detectors, which can be read out at the bunch crossing rate of a modern hadron collider such as the LHC. The SciFi tracker currently under construction for the LHCb experiment is a recent example [7].

On the other hand, the most advanced photodetection technology only mitigates some of the intrinsic limitations of the SciFi technology. The achievable spatial resolution is correlated with the fibre diameter and thus with the light yield, unless one conceives staggered multi-layer fibre arrangements which come at a cost in terms of the number of readout channel and material budget. A further limitation is the moderate radiation hardness of plastic scintillators which currently prevents or at least complicates their use in very harsh radiation environments.

1.2 Main characteristics and limits

The performance of a scintillating fibre based detector is often driven by the achievable signal amplitude A with its unavoidable (Poisson-like) statistical fluctuations σ_A. It affects parameters like detection efficiency, spatial resolution and energy resolution. For time critical applications the decay time constant of the scintillation light should be as short as possible. It allows for very high rate experiments, or in combination with a high signal amplitude, for high precision timing measurements.

The signal amplitude for a given energy deposit in the fibre ΔE can be factorised into (1) generation, (2) collection , (3) transport and (4) detection of the scintillation light.

$$A/\Delta E = Y_s \cdot \epsilon_{\text{coll}} \cdot \epsilon_{\text{trans}} \cdot PDE$$

where all factors are functions of the wavelength.

The ionisation light yield $Y_s(\lambda)$, measured in photons per deposited energy, is an intrinsic property of the scintillator. It depends on the choice of the core material and the additive dyes, the degree of spectral matching between the activator and wavelength shifting dyes and the quantum efficiency of the latter.

The light collection and transport are affected by the construction of the fibre (core geometry plus single or double cladding structure) and by the purity of the involved materials. The collection (sometimes also called trapping) efficiency ϵ_{coll} describes the fraction of the isotropically emitted scintillation light which falls into the two cones in which it undergoes total internal reflection. For double cladded fibres ϵ_{coll} is about 5.3% per hemisphere. The losses during the light transport through the fibre over a distance d are characterised by the wavelength dependent light attenuation length $\Lambda(\lambda)$, $\epsilon_{\text{trans}} = 1 - \exp(-d/\Lambda)$. Self absorption of the wavelength shifting dye, caused by an insufficient Stokes shift, can also reduce the transparency of the fibre.

The emission spectrum of the scintillator generally appears to shift towards the red during its transport through the fibre, as scatter and absorption phenomena in the fibre core affect shorter wavelengths more than longer ones. The effective emission spectrum at the end of the fibre should be optimally matched to the photon detection efficiency $PDE(\lambda)$ of the photodetector. Similarly, the degradation of the transparency of the fibre core which is observed after exposure of the fibre to ionising radiation, affects primarily the shorter wavelengths.

This article describes the first results of an ongoing R&D effort aiming at a significant performance gain of scintillating fibres, mainly in view of their use in high rate experiments which are typically also confronted with harsh radiation environments. The focus lies on the development of very fast and high yield scintillating fibres with emission spectra in the blue-green to green wavelength domains, well matched to the PDE spectrum of modern SiPM photodetectors, and less affected by radiation damage.

2017 JINST 12 P05013

The well established scintillating fibres of type SCSF-78 (blue) and SCSF-3HF (green), produced and commercialised by Kuraray[1] define the current state-of-the-art and serve as reference. They are made from a polystyrene (PS) core and employ a double cladding structure of polymethylmethacrylate (PMMA) and a fluorinated polymer. The thickness of each cladding layer is 3% of the total fibre diameter.

2 Development of high performance luminophores

From the materials point of view, scintillating fibres rely upon the composition of plastic scintillators, in which a polystyrene polymer matrix contains two types of organic luminophores: an activator and a spectral shifter. Following energy deposition by a charged particle, the polymer matrix emits primary UV photons. Since UV photons have very short attenuation length, they are further converted via step by step absorption and re-emission by the activator and spectral shifter luminophores into lower energy photons with larger attenuation length. The efficiency of a multi-step process is generally not very high.

Recently a new type of high performance luminophores called Nanostructured Organosilicon Luminophores (NOLs) was suggested [8]. They are based on covalent bonding of the activator and spectral shifter organic luminophores through Si atoms into a united branched or dendritic organo-silicon molecule - NOL. Silicon atoms in the NOL, on the one hand, break the conjugation between the organic luminophores attached to it, and, on the other hand, fix them on a small distance from each other without formation of excimers. The particular molecular structure of NOLs leads to a highly efficient non-radiative intramolecular energy transfer from the activator to the spectral shifter by Förster mechanism, and to faster down-shifting of the absorbed light. As a result, NOLs possess high molar absorption coefficients, large pseudo Stokes shift and high photoluminescense quantum yield combined with fast photoluminescense decay time, sometimes as small as 0.8–0.9 ns [9]. In addition, by choosing different organic luminophores for the synthesis of NOLs, both their absorption and emission spectra can be tuned to the desired regions [10]. NOLs are compatible with a range of optical polymers such as PMMA, PS or silicones [11] which allows for the creation of highly efficient plastic scintillators, spectral-shifting coatings or sheets. NOL-containing layers or optical plates have already been used for highly efficient down-shifting of light in various optoelectronic devices, such as organic light emitting diodes [12], thin film photovoltaics [13], elementary particles noble gas detectors [14] or pure CsI scintillators [15]. In this work, we report on our first results on the application of NOLs in highly efficient and fast scintillating fibres.

High scintillation yield in fibres requires a rather large concentration of the activator. However, long attenuation length can only be achieved by keeping the concentration of the spectral shifter relatively low. Therefore, pure NOLs are not expected to be efficient for scintillating fibres, as their ratio of activator to spectral shifter luminophores would be far from the optimum. Consequently, we have used here a conventional activator and added NOLs as highly efficient spectral shifters with high absorption cross-section and ultra-short photoluminescense decay time. For this purpose, we selected two different NOLs, which are able to absorb the emission coming from the activator

[1]Kuraray Co. Ltd., Tokyo, Japan

2017 JINST 12 P05013

luminophores, in particular: (1) NOL11 emitting in the blue region with maxima at 397, 421 and 445 nm, having photoluminescence quantum yield (PLQY) of 96% and photoluminescense decay time $\tau = 0.98$ ns, and (2) NOL19 emitting in the green region with maxima at 436, 466 and 490 nm, having PLQY = 87% and $\tau = 0.93$ ns.[2]

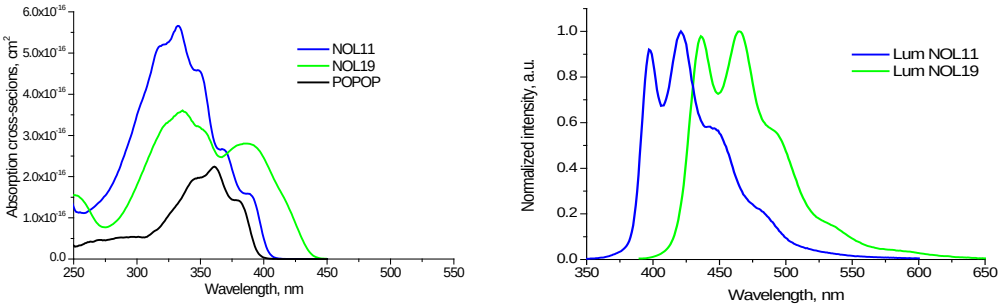

Figure 1. Absorption (left) and luminescence (right) spectra of NOL11 and NOL19 used as highly efficient spectral shifters in scintillating fibers BPF-11-1 and GPF-19-1. For comparison, the absorption spectrum of POPOP, often used as the spectral shifter in the standard plastic scintillators, is shown as well.

To characterize the intrinsic properties of the NOLs, the absorption and luminescence spectra of NOL11 and NOL19 were measured in diluted THF solution, as shown in figure 1. For comparison, the absorption spectrum of one of the standard spectral shifters used in plastic scintillators and scintillating fibres — POPOP — is included in the figure. As can be seen from this data, the integral absorption of both NOLs is about 3 times larger than those of POPOP. The absorption edge of NOL11 lies at 410 nm, while it is at 440 nm for NOL19. This difference in the absorption spectra of NOL11 and NOL19 as well as their internal molecular structure leads to a shift between the NOL11 and NOL19 luminescence spectra of about 45 nm. The first emission peaks of NOL11 and NOL19, at 397 and 436 nm, respectively, will be re-absorbed for high NOL concentrations or for large optical paths. Thus, NOL11 emits in the blue and NOL19 in the green regions. These two NOLs were used for the preparation of scintillating fibres, in the following called BPF-11-1 and GPF-19-1, respectively (Blue/Green Prototype Fibres 1).

3 Production of scintillating fibres

All fibres discussed here were made by a preform drawing method, developed by Kuraray. This production method is less efficient in productivity to an extrusion method used widely for ordinary optical plastic fibres, however it brings advantages when different low-volume productions for a wide range of applications are required, as it is typically the case for scintillating fibres.

The activator and NOLs were admixed to the styrene monomer and bulk-polymerised in a cylindrical vessel to a cylindrical core rod. In order to produce multi-cladding type fibres, the polymerized core was then dressed with two cladding cylinders, where the inner material was

[2]All these measurements were made in diluted THF solution to characterize the properties of individual NOLs. See catalogue at: http://www.luminnotech.com.

2017 JINST 12 P05013

PMMA and the outer a fluorinated polymer. This preform rod was then set in a heating furnace and drawn into thin fibre of 0.25 mm outer diameter. All fibres, NOL and reference fibres, presented here were multi-cladding type in order to maximise effective light yield and attenuation length.

Polystyrene is a polymer that easily deteriorates and discolours under the influence of oxygen and heat, leading to increased optical absorption in the wavelength region between 400 nm and 550 nm. To achieve maximum attenuation length, control of oxygen and heat is crucial, particularly as preform polymerisation and fibre drawing are high temperature processes.

A further important point concerns the molecular orientation of the polystyrene core polymer, which is determined by certain parameters of the fibre drawing process. A higher degree of molecular orientation benefits the mechanical strength of the fibre, but reduces its optical transparency, i.e. results in a shorter attenuation length. The fibre drawing process requires therefore a well-balanced and stable control of the involved parameters.

4 Performance characterisation

In the following we describe the performance of the two new prototype fibres. For each measurement we give a short description of the experimental set-up and compare the fibre to the SCSF-78 and SCSF-3HF reference fibres. All fibres discussed in this article have a diameter of 250 μm.

4.1 Spectral emission

The emission spectrum of a scintillating fibre depends primarily on the choice of the wavelength shifter and on the distance between the excitation point and the photodetector. In our set-up, which is described in detail in [16], the wavelength shifter in the fibre is excited by four UV-LEDs. Those are mounted in an integrating sphere-like cavity through which the fibre passes. The cavity is mounted on a carriage which can be moved along the fibre. The fibre is read out at one extremity by a spectrometer (Ocean Optics USB2000+UV-VIS-ES).

Figure 2 shows the emission spectra of the prototype fibres and of the reference SCSF-78 and SCSF-3HF fibres, excited at a distance of 15 cm, 95 cm and 295 cm from the spectrometer. Both SCSF-78 and BPF-11-1 are blue fibres with maxima in the region between 420 and 450 nm. The emission spectra of the GPF-19-1 and SCSF-3HF peak at 470 nm and 530 nm, respectively (green). The measurements presented in figure 2 show clearly the before mentioned shifting of the emission spectrum towards longer wavelength when the distance between excitation and detection point increases, i.e. the photons with shorter wavelength tend to be more attenuated than photons with longer wavelengths.

4.2 Attenuation length

The attenuation length $\Lambda(\lambda)$ characterises the quality of light transport through the fibre (see section 1.2). Alternatively, the attenuation coefficient $\alpha(\lambda) \equiv [\Lambda(\lambda)]^{-1}$ is used, e.g. in the context of radiation damage (see section 4.5).

As mentioned above, the set-up [16] used for the measurement of the attenuation length was the same as the one for the spectral emission, except that for integral measurements the spectrometer (Ocean Optics USB2000+UV-VIS-ES) was replaced by a Si-PIN photodiode (Newport 818-UV).

2017 JINST 12 P05013

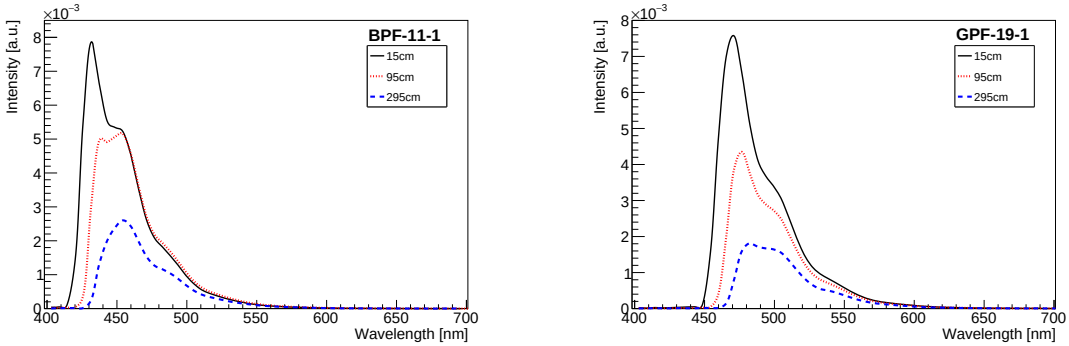

(a) BPF-11-1

(b) GPF-19-1

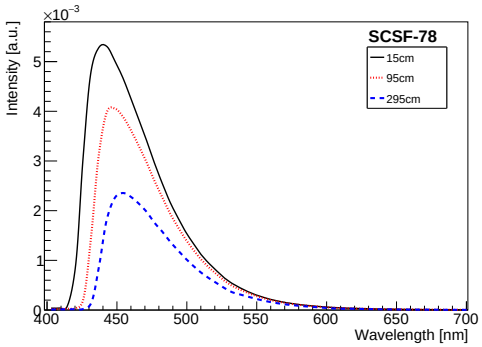

(c) SCSF-78

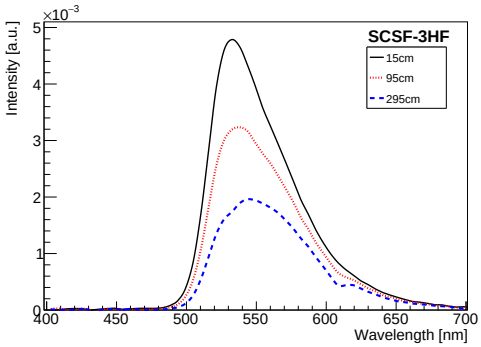

(d) SCSF-3HF

Figure 2. Emission spectra at distances of 15 cm, 95 cm and 295 cm, respectively, from the spectrometer.

The spectral attenuation length was derived from exponential fits to the intensities measured with the spectrometer in wavelength bins of about 5 nm, at different excitation distances from the spectrometer. The fits were performed between 100 and 300 cm, to avoid the contribution of a second exponential with shorter attenuation length due to losses of cladding light and to photons travelling with non-meridional trajectories inside the fibre. This steep exponential term has typical attenuation lengths of 20–30 cm, i.e. it is already sufficiently attenuated at 100 cm to be ignored.

The results of the spectral attenuation length presented in figure 3 show that the SCSF-78 fibre outperforms the other samples in the wavelength region 430 – 600 nm, i.e. where its emission spectrum lies, while the SCSF-3HF is favoured at higher wavelengths, where the other samples do not emit any light. In general the photons with longer wavelengths are less attenuated in the fibre, with the exception of the two minima at $\lambda \sim 535$ nm and $\lambda \sim 610$ nm. The enhanced absorption in these regions can be assigned to the excitation of high harmonics of the aromatic C-H stretching vibration levels of polystyrene [17] and are therefore visible in all four samples.

The integral attenuation length was measured in a similar way. An exponential fit was applied to the recorded intensities of the Si-PIN photodiode at different excitation distances. As discussed in [16], the precision on Λ with the set-up used is 5%. Unless the sensitivity of the used photodetector is constant in the wavelength range of the detected photons, the integral attenuation length will depend on the spectral sensitivity of the photodetector. As shown in figure 4,

2017 JINST 12 P05013

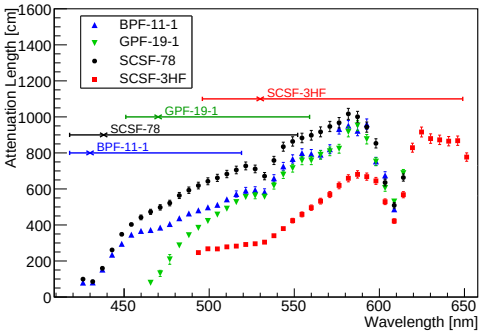

Figure 3. Spectral attenuation length. For each sample the crosses on the horizontal bars correspond to the wavelength of maximum emission intensity I_{max}, while the bars extend over the wavelength region where $I(\lambda) \geq 0.05 \cdot I_{max}$.

the quantum efficiency of the used Si-PIN diode increases steadily from 0.5 at 400 nm to 0.84 at 650 nm. The SCSF-3HF sample particularly profits from the enhanced sensitivity of the photodiode at longer wavelengths and achieves an integral attenuation length comparable to the SCSF-78 fibre (see figure 5). Both reference fibres show integral attenuation lengths exceeding 300 cm ($\Lambda_{SCSF-78} = 351$ cm; $\Lambda_{SCSF-3HF} = 330$ cm), while the attenuation lengths of the prototype fibres are both smaller than 300 cm ($\Lambda_{BPF-11-1} = 263$ cm; $\Lambda_{GPF-19-1} = 294$ cm).

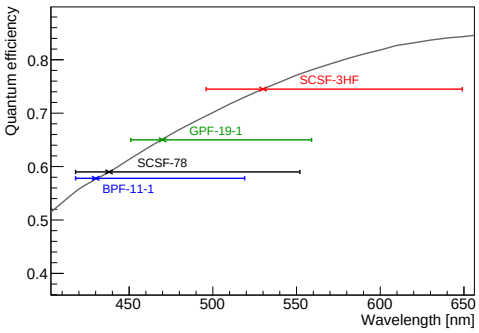

Figure 4. Sensitivity of the Si-PIN photodiode Newport 818-UV. For each sample the crosses on the horizontal bars correspond to the maximum emission intensity I_{max}, while the bars extend over the wavelength region where $I(\lambda) \geq 0.05 \cdot I_{max}$.

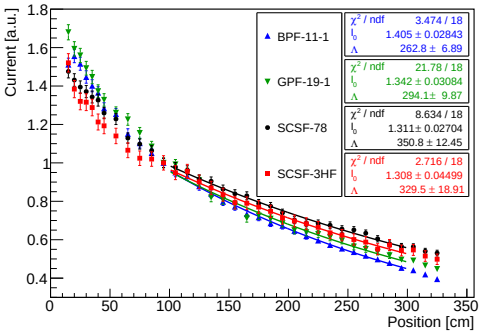

Figure 5. Fits to determine the integral attenuation length. The measured intensities are normalised here, such that the intensity at 95 cm is equal to 1.

4.3 Ionisation light yield

The measurement of the intrinsic ionisation light yield of thin scintillating fibres is a challenge as it requires knowledge of the energy deposited by a charged particle (or high energy photon) in the fibre core and many other parameters such as the trapping efficiency of the fibre, the quality of coupling between fibre and photodetector or the photon detection efficiency of the latter. Typical values in the literature lie around 7000–10000 photons/MeV. However, for the purpose of comparing the

2017 JINST 12 P05013

prototype fibres among each other and with the reference fibres it is sufficient to perform a relative measurement under reproducible and well defined experimental conditions. Our method is based on the measurement of the light output at the end of the fibre, in units of photoelectrons (p.e.) detected by a photodetector, created by a minimum ionising particle traversing the fibre at a given distance from the detector. A more detailed description of the set-up and its components can be found in [18]. The whole set-up is placed inside a dark room at an ambient temperature of about 22 °C.

In order to increase the measured light output and therefore the signal to noise ratio we arranged the three test fibres and two trigger fibres in a way that the ionising particle had to traverse all three fibres. The three test fibres of 250 μm diameter and 2.6 m length were read out jointly by a single Silicon Photomultiplier (SiPM type Hamamatsu S13360-1350CS). The average path length of the particles through the active part of the fibres was calculated to be 0.52 mm. On one end the fibres were glued into a cylindrical plastic ferrule and then cut with a diamond milling tool in order to achieve a good quality end cut. The other end was left unmachined. The SiPM was connected to a Hamamatsu C12332-01 driver board featuring a temperature compensation of the bias voltage and signal amplification. Two trigger fibres with the same diameter, placed on top and below the fibres under test, were read out individually by two Hamamatsu H7826 Photomultiplier Tubes (PMTs). The ionising particles were provided by a special monochromatic electron gun [18], based on a Sr-90 source, placed below the fibres, which allows to select electrons with an energy of 1.1 ± 0.1 MeV using a magnetic field and collimators. Electrons of 1.1 MeV can be considered as minimum ionising particles (MIP). The SiPM signal was readout with a LeCroy LT344 digital oscilloscope (bandwidth 500 MHz, 500 MS/s)). The respective trigger signal was generated as a coincidence of the amplified and discriminated trigger PMT signals, leading to a trigger rate of about 10 Hz. The trigger ensures that only electrons traversing all three test fibres were recorded. After pedestal subtraction, the mean accumulated signal charge was converted into photoelectrons after appropriate calibration using single photoelectron spectra.

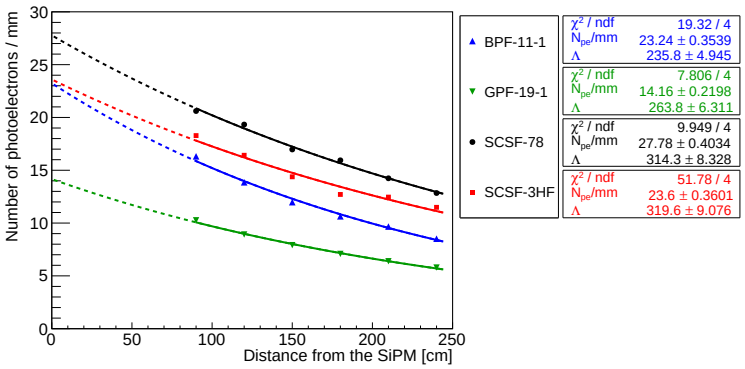

Figure 6. Light yield of prototype fibre samples and comparison to Kuraray standard fibres SCSF-78 and SCSF-3HF. The error bars are covered by the markers. The systematic uncertainty for the measurement was found to be 2.5 % and should be added to the above errors obtained from the fits.

We measured the light output at distances $d = 90$ cm to $d = 240$ cm from the SiPM in steps of 30 cm and normalised it to the average pathlength of 0.52 mm. Finally the data points were fitted by a single exponential function $\left(f(d) = N_{\mathrm{pe}} e^{-d/\Lambda}\right)$. The scintillation yield was defined as

2017 JINST 12 P05013

the light output extrapolated to $d = 0$. It can be noted that such measurement allows also to extract the attenuation length Λ using a different method than the one described in section 4.2. Figure 6 shows the results of the light yield measurements for the two prototype fibres and Kuraray standard fibres. We obtained a value of $N_{pe} = 23.2$/mm for the blue prototype fibre (BPF-11-1), reaching almost 85% of the best value achieved with the blue emitting standard fibre SCSF-78 ($N_{pe} = 27.8$/mm). We believe that the BPF-11-1 light yield can be further enhanced by optimising the activator and wavelength shifter concentrations. The green prototype fibre (GPF-19-1) yields at this stage $N_{pe} = 14.2$/mm, i.e. about 40% less than the reference fibre SCSF-3HF ($N_{pe} = 23.6$/mm). It should be noted that we experienced some unstable conditions during the fibre drawing process for this particular fibre which may have deteriorated its performance.

4.4 Decay time

For fast timing applications it is of particular importance that the decay time constant of a scintillating fibre is as low as possible. The described measurement method is based on the assumption that the decay time of the wavelength shifting dye dominates the overall decay time of the scintillating fibre. A fast pulsed UV-LED (PicoQuant PLS370, $\lambda = 375$ nm, $\sigma \sim 220$ ps pulse width) was used to laterally excite a single fibre at a distance of about 10–15 cm from one fibre end which was attached to a fast PMT (Hamamatsu H7826). The fibre was machined with a diamond milling tool in order to achieve a good quality end cut. The light intensity was adjusted such that the PMT detected primarily single photons. A pulse generator drove the LED and provided the start signal, whereas the amplified and discriminated (threshold 0.5 p.e.) PMT signal gave the stop signal for each single event. For each measurement typically a few 100k events were recorded using a LeCroy LT344 digital oscilloscope. The resulting time distributions can be well described by an exponential function containing the decay time constant τ of the scintillation light, convoluted with a Gaussian with a width of $\sigma \sim 450$ ps accounting for the overall time jitter of the experimental set-up, given by:

$$f(x;\mu,\sigma,\tau) = \frac{1}{2\tau}\exp\left[\frac{1}{2\tau}(2\mu + \frac{\sigma^2}{\tau} - 2x)\right]\operatorname{erfc}\left(\frac{\mu + \frac{\sigma^2}{\tau} - x}{\sqrt{2}\sigma}\right) \tag{4.1}$$

where erfc is the complementary error function.

Figure 7 shows the measured and fitted time distributions for the prototype and reference fibres. The decay time constants of 2.4 ns and 6.2 ns obtained for the blue and green reference fibres, respectively, are in good agreement with the catalogue values of 2.8 ns and 7 ns for SCSF-78 and SCSF-3HF provided by Kuraray.[3] The measurements of the prototype fibres yield a decay time of 1.2–1.3 ns which is about a factor two faster than the best standard fibre and demonstrates the potential of using NOLs for very fast scintillating fibres.

4.5 Performance degradation after x-ray irradiation

An X-ray set-up [19], based on an X-ray tube equipped with a tungsten target, allowed to uniformly irradiate 3.5 m long fibre samples. For this test the tube was operated at 40 kV and at an anode

[3] www.kuraraypsf.jp; it should be noted that the Kuraray catalogue value of the decay time constant of SCSF-78 is not based on a direct measurement of a fibre but derived from the decay time of the wavelength shifter dye of this fibre in solution.

2017 JINST 12 P05013

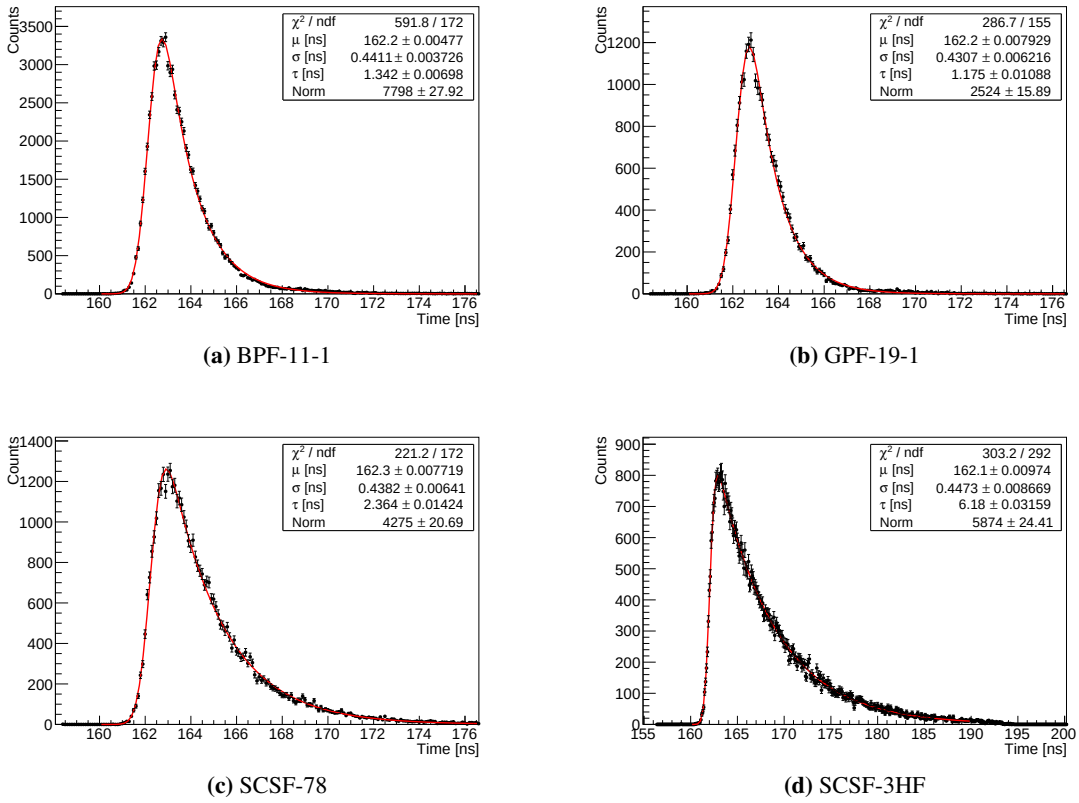

(a) BPF-11-1 **(b)** GPF-19-1

(c) SCSF-78 **(d)** SCSF-3HF

Figure 7. Decay time of prototype (top) and reference fibres (bottom).

current of 30 mA. With these settings the fibres under test were irradiated to a dose of 1 kGy in 45 minutes (dose rate of 23 Gy/min).

The quantity used to assess the damage caused by the irradiation is the additional attenuation coefficient α_{rad}. It is defined as $\alpha_{\text{rad}} \equiv \alpha' - \alpha_0$, where $\alpha_0 \equiv \Lambda_0^{-1}$ is the intrinsic attenuation of the fibre and $\alpha' \equiv \Lambda'^{-1}$ is the attenuation after the irradiation.

It should be noted that the performance degradation of a fibre after irradiation with X-rays does not necessarily allow to infer the damage obtained from other radiation sources. In particular hadron irradiation causes not only a higher deterioration just after the irradiation, but also the time evolution of the damage is different: while hadron irradiation induces a permanent damage, the fibres irradiated with X-rays completely anneal, typically on a time scale of weeks. The time constant of the annealing may vary depending on the choice of the dyes. For example, for the SCSF-78 fibres we observe a total annealing after about 1 month from the irradiation. The results of the X-ray irradiations are shown in figures 8 to 10. The measurement of α' was performed just after the irradiation and then repeated a week later. The blue fibres (SCSF-78 and BPF-11-1) are less damaged than the green fibres (GPF-19-1 and SCSF-3HF). The spectral analysis shows how the resistance to X-rays depends on the chosen dyes. The two blue fibres behave similarly, both after the irradiation and after the annealing, with a more or less pronounced minimum in the wavelength region around 500 nm. The green fibres are equally affected only for wavelengths up to 540 nm,

2017 JINST 12 P05013

while they exhibit different behaviours in the range 540 – 600 nm. The SCSF-3HF sample shows a faster annealing than GPF-19-1. The irradiation of the fibres and the consequent annealing took place in normal laboratory atmosphere at room temperature.

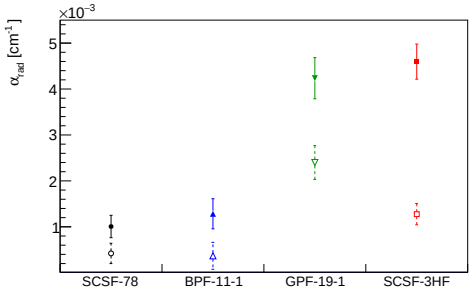

Figure 8. Additional attenuation coefficient after X-ray irradiation $\alpha_{\text{rad}} \equiv \alpha' - \alpha_0$. For each sample, α_0 has been measured before irradiation, while α' is the attenuation directly after irradiation (filled markers) and after 7 days of annealing (empty markers).

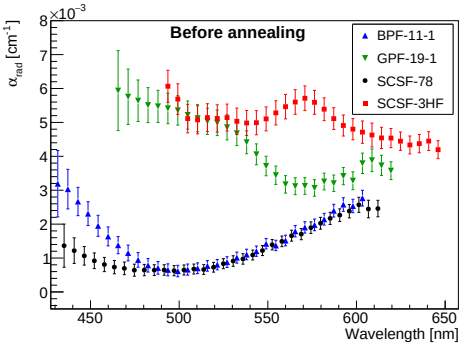

Figure 9. Additional attenuation coefficient directly after X-ray irradiation.

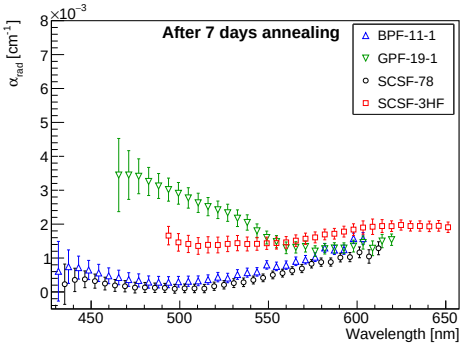

Figure 10. Additional attenuation coefficient after 7 days of annealing.

5 Discussion

The results presented in this work are summarised in table 1. They reflect an intermediate state of an ongoing development programme. Both the blue and the green prototype fibres show a very short decay time constant and mark to our knowledge new records. The GPF-19-1 prototype fibre is about a factor 6 faster than the SCSF-3HF fibre produced by Kuraray and about two times faster than the green BCF-20 fibre produced by Saint-Gobain Crystals.[4]

At identical number of detected photoelectrons, the decay time constant τ impacts linearly on the achievable time resolution or coincidence resolving time $\sigma_t \propto \tau$. An example where such reduced decay time may boost the detector performance is the Mu3e experiment at PSI [20, 21].

[4]Saint-Gobain Crystals, Hiram, Ohio, U.S.A.

2017 JINST 12 P05013

Table 1. Summary of fibre performance. The peak wavelength λ_{peak} is for fibre excitation close to the photodetector.

Fibre type	λ_{peak} [nm]	Λ [cm]	LY [p.e./mm]	τ [ns]
BPF-11-1	430	263	23.2	1.34
GPF-19-1	470	294	14.2	1.18
SCSF-78	440	351	27.8	2.36
SCSF-3HF	530	330	23.6	6.18

A fast scintillating fibre hodoscope is foreseen to discriminate combinatoric background from $\mu^+ \to e^+ \bar{\nu_\mu} \nu_e$ decays against the lepton flavour violating signal channel $\mu^+ \to e^+ e^- e^+$. Given the small length of the detector (36 cm) the not yet optimal attenuation length of our prototype fibres would not lead to noticeable performance loss.

We expect that further optimisation of the luminophore concentrations as well as of the production process will lead to significantly longer attenuation length and increased scintillation yield. The goal is to reach a 20% higher scintillation yield than the SCSF-78. Such fibres would be highly attractive for the large LHCb SciFi Tracker [7] currently under construction at CERN. The experiment would particularly profit from a fast blue-green fibre with high light yield and long attenuation length.

The LHCb SciFi Tracker uses 250 μm SCSF-78 fibres of 2.5 m length, read out at one end with SiPM photodetectors while the other fibre end is mirrored. Given that the attenuation length of polystyrene generally increases with wavelength, a blue-green fibre could be an advantage. Peak emission around 500 nm would very well match the spectral sensitivity of the SiPM detectors. In the inner region, close to the LHC beam pipe the fibres are exposed to an ionising dose of up to 35 kGy, accumulated over the lifetime of the detector. This leads gradually to a reduction of the attenuation length and hence to a lower number of detected photoelectrons, ultimately affecting the hit efficiency of the detector. The problem could be mitigated by using fibres with an initially higher scintillation yield, provided that they show the same radiation damage.

The fibre length of 2.5 m leads to a substantial spread of the photon propagation times of up to 15 ns, for reflected photons of even up to 30 ns ($2 \cdot 2.5$ m $\cdot$ 6 ns/m). Fluctuations due to the decay time of the scintillator come on top. Fibres with significantly shorter decay time mitigate the problem that a fraction of the scintillation light spills over in the next LHC bunch crossing following with a 25 ns interval.

The irradiation tests with X-rays to a dose of 1 kGy indicate that the radiation damage of the blue BPF-11-1 and the green GPF-19-1 fibres are on a level comparable to the respective reference fibres, however irradiation tests with hadrons and to higher doses still have to be performed.

It should be noted that the NOL principle on which the discussed scintillating prototype fibres are based, can also be applied to scintillator tiles [8] and wavelength shifting (WLS) fibres which should potentially be very fast and efficient. The requirements are however different, as WLS fibres shall not produce scintillation light, i.e. the absorption spectrum of the luminophore must not overlap with the emission spectrum of polystryrene.

2017 JINST 12 P05013

6 Outlook

The prototype fibres discussed in this article represent an intermediate step of an ongoing development programme. Further iterations, optimising luminophore choices and concentrations as well as the process steps, are expected to improve the performance in several respects.

Given the novelty of NOLs, little is known about the long term stability of NOL-based fibres. In general, the oxidation stability of NOLs is similar or slightly higher than the one of normal organic dyes. We therefore don't expect any degradation of NOL fibres in a normal ambient environment. Sustained exposure to light is known to damage scintillating fibres. Quantitative tests need to be performed by exposing fibre samples to various light sources and monitoring their performance. Applications in modern particle physics experiment will often entail exposure to harsh (multi-kGy) radiation fields, typically consisting of multi-GeV hadrons. We will therefore complement our studies with x-rays by high energy hadrons, which are known to produce permanent damage in the fibres. The CERN PS irradiation facility providing intense proton beams of 23 GeV/c is well suitable for such a campaign.

Acknowledgments

We are grateful to our colleagues from the LHCb collaboration for their interest and continuing support of this development.

References

[1] R.C. Ruchti, *The use of scintillating fibers for charged-particle tracking*, *Annu. Rev. Nucl. Part. S.* **46** (1996) 281.

[2] C. Joram, G. Haefeli and B. Leverington, *Scintillating Fibre Tracking at High Luminosity Colliders*, 2015 *JINST* **10** C08005.

[3] M. Adinolfi et al., *The KLOE electromagnetic calorimeter*, *Nucl. Instrum. Meth.* **A 482** (2002) 364.

[4] R. Wigmans, *Calorimetry*, Oxford University Press (2000).

[5] E224 collaboration, J.K. Ahn et al., *Search for the H dibaryon in (K-,K+) reaction with scintillating fiber active target*, *Phys. Lett.* **B 378** (1996) 53.

[6] D. Renker and E. Lorenz, *Advances in solid state photon detectors*, 2009 *JINST* **4** P04004.

[7] LHCb collaboration, *LHCb Tracker Upgrade*, Technical Design Report, CERN-LHCC-2014-001.

[8] S.A. Ponomarenko et al., *Nanostructured organosilicon luminophores and their application in highly efficient plastic scintillators*, *Sci. Rep.* **4** (2014) 6549.

[9] T.Yu. Starikova et al., *A novel highly efficient nanostructured organosilicon luminophore with unusually fast photoluminescence*, *J. Mater. Chem.* **C 4** (2016) 4699.

[10] S.A. Ponomarenko et al., *Nanostructured organosilicon luminophores as a new concept of nanomaterials for highly efficient down-conversion of light*, *Proc. SPIE* **9545** (2015) 954509.

[11] M.S. Skorotetcky et al., *Novel Cross-Linked Luminescent Silicone Composites Based on Reactive Nanostructured Organosilicon Luminophores*, *Silicon* **7** (2015) 191.

2017 JINST 12 P05013

[12] Y.N. Luponosov et al., *Nanostructured Organosilicon Luminophores for Effective Light Conversion in Organic Light Emitting Diodes*, *Org. Photonics Photovolt.* **3** (2015) 148.

[13] T. Uekert et al, *Nanostructured organosilicon luminophores in highly efficient luminescent down-shifting layers for thin film photovoltaics*, *Sol. Energ. Mat. Sol. C.* **155** (2016) 1.

[14] D.Yu. Akimov et al., *Development of VUV wavelength shifter for the use with a visible light photodetector in noble gas filled detectors*, *Nucl. Instrum. Meth.* **A 695** (2012) 403.

[15] Y. Jin, H. Aihara, O.V. Borshchev, D.A. Epifanov, S.A. Ponomarenko and N.M. Surin, *Study of a pure CsI crystal readout by APD for Belle II end cap ECL upgrade*, *Nucl. Instrum. Meth.* **A 824** (2016) 691.

[16] C. Alfieri et al., *A set-up to measure the optical attenuation length of scintillating fibres*, CERN-LHCb-PUB-2015-011.

[17] T.Kaino, M. Fujiki and S. Nara, *Low loss polystyrene core optical fibers*, *J. Appl. Phys.* **52** (1981) 7061.

[18] C. Alfieri et al., *An experimental set-up to measure Light Yield of Scintillating Fibres*, CERN-LHCb-PUB-2015-012.

[19] L. Gavardi et al., *A setup to perform X-ray irradiation tests on scintillating fibres for the SciFi project*, CERN-LHCb-PUB-2017-008.

[20] A. Blondel et al., *Research Proposal for an Experiment to Search for the Decay $\mu \to eee$*, arXiv:1301.6113.

[21] N. Berger, *The Mu3e Experiment*, *Nucl. Phys. (Proc. Suppl.)* **B 248–250** (2014) 35.

2017 JINST 12 P05013